Brownian motion of colloidal particles in a model porous medium

G. Viramontes-Gamboa, M. Medina-Noyola, and J. L. Arauz-Lara

Instituto de Física "Manuel Sandoval Vallarta," Universidad Autónoma de San Luis Potosí, Alvaro Obregón 64, 78000 San Luis Potosí, San Luis Potosí, Mexico

The motion of interacting colloidal particles diffusing in a model porous medium is studied by means of computer simulations using a Brownian dynamics algorithm. The particles are assumed to interact through a repulsive Yukawa pair potential. The porous medium is formed by a fraction of the colloidal particles whose positions are frozen in a given spatial configuration. Varying the molar fraction of the mobile particles, keeping constant the total particle concentration, and/or varying the parameters of the pair potential, we vary the effective porous medium in which the mobile particles diffuse. Here we report results for the mean squared displacement of the mobile particles for different values of their molar fraction and of the Yukawa amplitude. We compare our results with theoretical calculations from two independent approaches to the description of tracer diffusion in colloidal mixtures, by considering the case, in both theories, in which a fraction of the particles has vanishing free-diffusion coefficient. We find that both theories predict the same basic qualitative trends for the mean squared displacement obtained from the Brownian dynamics experiments. For completeness, we also present the static structure of the colloidal suspension permeating our model porous medium.

PACS number(s): 82.70.Dd, 05.40.+j

I. INTRODUCTION

Porous materials represent an important and interesting class of systems [1]. Their technological relevance spans a wide range of applications [1,2], which demand the investigation of many issues such as their structure and morphology [1,3,4] and the equilibrium [5,6] and transport [7-9] of systems, such as liquids, that permeate their porous structure. The description of the static but random morphology of a porous material has been approached, from the experimental side, by means of conventional scattering techniques [1], whereas from the theoretical point of view, new concepts and properties have to be identified to describe the relevant features of the random interpenetrating solid and porous domains [3,4]. This random structure is then the stage in which interesting dynamic and thermodynamic processes can take place when the porous domain is filled by a fluid. Given the variety of issues that may be of interest, it is not surprising that no simple and universal model or approach is available to describe them within a unified theoretical framework. Thus, whereas some models focus, for example, on the statistical mechanics or the transport properties of the permeating fluid in the interior of a single pore of a given (planar or cylindrical) geometry, or even on arrays of connected pores of such a geometry [8], other models incorporate at the outset the spatial randomness of the system [6,9]. One model of the latter class is that of a partially quenched fluid mixture in which the kinetic energy of one species is totally quenched, thus freezing its structure to mimic the porous matrix. The other species (i.e., the fluid formed by the mobile particles) is then allowed to equilibrate in the static field of the matrix. To describe the average structure of the fluid permeating this model porous matrix, approaches such as Mayer expansions and integral equation methods have been applied and simulation results have been reported [6].

In this paper we report a more extensive account of the results of our work [10] on a Brownian dynamics version of essentially this model. We focus on some specific dynamic phenomenon, namely, the tracer diffusion of labeled Brownian particles, and on its dependence on the structure of the matrix and on the interactions of the Brownian fluid particles among themselves and with the matrix. These dynamic properties also depend on the detailed dynamic laws governing the motion of the mobile fluid particles. In this regard, our work is based primarily on a computer simulation experiment generated by the Brownian dynamics algorithm employed to simulate the random motion of colloidal particles suspended in a liquid solvent [11,12]. Thus the closest practical experimental realization of our model is that of a colloidal suspension permeating a porous material, such as in a chromatographic column. At this stage, however, we are not interested in addressing the complexity involved in the modeling of a particular experimental condition. Instead, we introduce a number of simplifications and idealizations that will allow us to focus on only a few well-defined (we believe) and general theoretical questions.

The computer simulation experiment we have performed is the following. The system consists of N_1 particles of species 1 and N_2 particles of species 2 in a three-dimensional cubic cell of volume V with periodic boundary conditions. These particles interact through a radial pair potential denoted by $u_{\alpha\beta}(r)$, where the indices α and β refer to species (1 or 2). The motion of the $N = N_1 + N_2$

particles is governed by the Brownian dynamics (BD) algorithm of Ermak and McCammon [11], without hydrodynamics interactions. This algorithm essentially solves the Smoluchowski equation for the N particles in the absence of external forces. This is also equivalent to the solution of N Langevin equations with the inertial terms neglected and coupled to each other through the interparticle forces. The free Brownian motion of particles of each species is determined by the free-diffusion coefficients D_1^0 and D_2^0. Freezing a certain configuration of the second species will be achieved by setting $D_2^0 = 0$ at a certain point in the simulation. For simplicity, in the results reported here, the N particles will be considered identical with respect to the interaction, which will be taken to be a Derjaguin-Landau-Verwey-Overbeek (DLVO) -type pair potential, i.e.,

$$\beta u_{\alpha\gamma}(r) = \beta u(r) = \begin{cases} K\dfrac{e^{-z[(\frac{r}{\sigma})-1]}}{(\frac{r}{\sigma})}, & r > \sigma \\ \infty, & r < \sigma, \end{cases} \quad (1.1)$$

where $\beta = (k_B T)^{-1}$, T is the temperature, and k_B is Boltzmann's constant. In Eq. (1.1), σ is the hard-sphere diameter of each of the N particles. The asymmetry between the two species is thus defined by the difference between D_1^0 and D_2^0, which are hence not related to σ; they are fixed independently, as we explain below. Also, here we shall restrict ourselves to the high-coupling regime, i.e., that in which the pair potential at contact measured in units of $k_B T$ is large. In fact, we shall restrict K to values in the range $100 \leq K \leq 500$. Under these conditions, the hard-sphere diameter σ will only play the role of an arbitrary length scale, which we take to be much smaller than the Debye screening length $(\frac{\sigma}{z})$ and the mean interparticle distance $l \sim n^{-1/3}$ $(n = N/V)$. Here the dimensionless screening constant z will be taken to be fixed, at a value $z = 0.15$, and we will restrict the total concentration to values of $n = n_1 + n_2$ (where $n_\alpha = N_\alpha/V$) such that the total volume fraction $\phi = \phi_1 + \phi_2$ (with $\phi_\alpha = \frac{\pi}{6}n_\alpha\sigma^3$) remains fixed at a value $\phi = 4.4 \times 10^{-4}$. In this manner, we shall only consider changes in the coupling parameter K and in the relative concentration of mobile to fixed particles, represented by the "mole fraction" of species 2, $x_2 = n_2/n$. As stated above, here we shall focus on essentially one fundamental property describing the Brownian motion of the mobile particles, namely, their mean squared displacement (MSD). Furthermore, we shall make no attempt to determine or estimate the asymptotic long-time value of the tracer-diffusion coefficient; instead, we shall mainly study the initial relaxation of the time-dependent diffusion coefficient. In this manner, we expect to understand some features of the tracer diffusion of labeled particles of a Brownian liquid permeating a frozen matrix $(x_2 \neq 0)$ by means of its comparison with the phenomenon of self-diffusion in model colloidal suspensions $(x_2 = 0)$ which has been widely studied in recent years [13–16]. The general condition interpolating between the two interesting limiting cases $(x_2 = 0$ and $x_2 = 1)$ will then involve simultaneously the interactions of the tracer particle with the rigid matrix and with the other mobile particles.

Although no simple theory has been developed to provide a fundamental theoretical interpretation of the phenomena described by our computer simulation experiment, here we discuss the results of extrapolating two theories developed in our group to describe tracer diffusion in colloidal mixtures in thermodynamic equilibrium. These theories have been shown to provide a satisfactory description of this phenomenon for the conditions for which they were formulated and its application in the present conditions is aimed only at determining the regimes in terms of time, composition, or coupling, at which their predictions remain reasonably accurate. Since the application of these theories will be based on a simplifying assumption regarding the static structure of the system, we also present some results for these properties. This is done in Sec. III, after describing the simulation experiment in Sec. II. In Sec. IV the results of this experiment for the dynamic properties are presented and discussed. In Sec. V we describe the two theories referred to above and compare their predictions with the simulation results. A final discussion and summary of this work is found in Sec. VI.

II. BROWNIAN DYNAMICS SIMULATION

The BD simulation starts from an arbitrary configuration $\mathbf{r}_i(0)$ $(i = 1, 2, ..., N)$, where $\mathbf{r}_i(t)$ is the position of particle i at time t. In the first stage of our simulation, each particle moves with the same free-diffusion coefficient, i.e., $D_1^0 = D_2^0 = D^0$. This stage goes as long as the system equilibrates and hence it is identical to the BD simulation of a monodisperse model colloidal suspension without hydrodynamic interactions. Simulations of this type and precisely for the same pair potential and a similar range of parameters have been reported in the literature [12]. Furthermore, their results have been quite useful not only for its comparison with theoretical predictions of some static and dynamic properties [13–16] but also in the interpretation of specific experimental results [17]. It is for this reason that we employ the DLVO potential above, so that we can establish some comparison with conditions widely studied and reported in the literature.

The second stage of our computer experiment starts, once the system has equilibrated, at the moment that we set $D_2^0 = 0$ and leave $D_1^0 = D^0$. That is, we freeze the position of the N_2 particles of species 2 and let the other N_1 particles continue their Brownian motion, still interacting among themselves and with the field of the N_2 immobile particles, which now constitute the porous matrix. This second stage continues until the Brownian fluid (i.e., the N_1 mobile particles) equilibrates in the static field of the matrix. In the case in which the ratio of mobile to fixed particles was not too small, this turned out to be a relatively short time. When this ratio was close to zero, this stage required a longer time due to the need of the tracer particles to search for its closest region of minimum energy in the simulation cell. In any case, averages were performed once an equilibrium was reached.

In this work we restrict ourselves to the description of tracer-diffusion properties of the fluid particles. The basic property we discuss here is the mean squared displacement $W(t) \equiv \langle [\Delta \mathbf{r}(t)]^2 \rangle / 6$ or, equivalently, the time-dependent self-diffusion coefficient $D(t)$, defined as

$$D(t) \equiv \frac{W(t)}{t} = \langle [\Delta \mathbf{r}(t)]^2 \rangle / 6t. \qquad (2.1)$$

To simplify the discussion of our results, we have chosen only a few illustrative cases. As described above, the parameters defining the system and its state are z, K, n, and x_2 and we shall keep the values of z and n fixed. Under these conditions, varying K turns out to be equivalent to varying the intensity of the interparticle repulsion and hence the effective diameter of the interaction between the particles. This means that increasing K will produce similar effects to increasing the total concentration. Thus, in what follows we present results for different values of the coupling parameter K and the mole fraction x_2.

For fixed K, we must distinguish three regimes in terms of the value of x_2: (i) $x_2 \approx 0$, corresponding to the virtual absence of fixed particles; (ii) $x_2 \approx 0.5$, in which roughly half of the particles move and the other half constitute the matrix; and (iii) $x_2 \approx 1$, in which case all the particles belong to the matrix, through which a negligible trace of mobile particles diffuse independently of each other. The first regime corresponds to ordinary self-diffusion, widely studied in the literature [16]. The second regime corresponds to the typical conditions on which we wish to focus, namely, that in which a fluid of interacting Brownian particles at nonzero concentration permeates a rigid matrix of fixed particles. The third regime corresponds to a particular interesting limiting condition of the previous case.

III. STATIC STRUCTURE

Although the main questions we want to address in this work refer to the tracer-diffusion properties, it is convenient at this point to mention some observations regarding the static structure of our model system under the specific, idealized conditions of our computer experiment. As explained above, before the position of the particles of species 2 are frozen, our system is just a monodisperse Brownian fluid in thermodynamic equilibrium. As such, it is an ergodic system and its thermodynamic and structural properties are well defined averages that can be calculated in the conventional manner [18]. For example, the radial distribution function (RDF) $g(r)$ corresponding to such conditions is presented in Fig. 1 (open circles) for three different values of the Yukawa amplitude, namely, $K = 100, 300$, and 500. If in this monodisperse liquid we imagine N_1 particles as pertaining to one "species" and N_2 particles to a second species, as in a true mixture, we can talk of various radial distribution functions [19] $g_{\alpha\beta}(r)$ ($\alpha, \beta = 1, 2$). In this case, however, it is obvious that $g_{11}(r) = g_{12}(r) = g_{22}(r) = g(r)$ since there is no real difference between the two species. In

our experiment, however, after we freeze the position of the particles of species 2, the other species is allowed to equilibrate in the presence of the fixed particles, which remain in a frozen spatial configuration. We can now calculate the RDF of the mobile particles $g_{11}(r)$ and the RDF $g_{12}(r)$ of the fixed particles around a mobile particle. The question arises whether these two RDF's are related to each other and to the RDF $g(r)$ of the monodisperse liquid before freezing one species. Of course, for $x_2 = 0$, since no particles were stopped, the answer is that $g_{11}(r) = g(r)$. For $x_2 \neq 0$, Fig. 1 answers this question from the point of view of our simulation results. There we compare $g_{11}(r)$ and $g_{12}(r)$ with $g(r)$ for $x_2 = 0.5$ and $x_2 = 1$ and the answer can be said to be $g_{11}(r) \approx g_{12}(r) \approx g(r)$. Let us mention, however, that the results for $g_{11}(r)$ and $g_{12}(r)$ correspond to an average over different configurations of the matrix of fixed particles (around 10 or 20 for $x_2 \approx 0.5$ and around 200 for $x_2 \approx 1$). This observation will be useful when we attempt a theoretical analysis of the dynamic results that follow.

IV. TRACER-DIFFUSION AVERAGES AND SIMULATION RESULTS

Just as we had to perform the averages leading to $g_{11}(r)$ or $g_{12}(r)$, when there is a finite concentration of obstacles ($x_2 \neq 0$), a similar procedure can be followed to evaluate the mean squared displacement of the mobile particles, which otherwise would depend on the spatial configuration of the frozen matrix. This is illustrated in Fig. 2, where we plot $D(t)$ for $x_2 = 0.5$ and $K = 100$ and 500. For each case, we show about ten different curves, clustered around a well-defined average value (solid lines). Each curve is the result of averaging the squared displacement $[\mathbf{r}_\alpha(t + \tau_0) - \mathbf{r}_\alpha(\tau_0)]^2$ over many possible initial times τ_0 along the trajectory of a given mobile particle ("time" average) and over the trajectories of each of the mobile particles $\alpha = 1, 2, ..., N_1$ ("ensemble" average), but for a given configuration of the fixed particles constituting the porous matrix. Repeating this experiment involves a different configuration of the matrix. Due to the finite size of the system, the resulting averages differ and each of the ten curves around the solid lines corresponds to a different matrix configuration. The dispersion, however, is not large, as observed in Fig. 2. An average that does not depend on the configuration of the matrix could be obtained by increasing the size of the simulation cell, but this is computationally more inconvenient than obtaining a set of curves, such as those in Fig. 2, and then averaging over them. The result is the solid lines in Fig. 2 and this is what we shall present from now on as the final average. We found that this is a very well-defined and representative average. Thus, if instead of averaging over the ten different curves we took a smaller number, let us say five, chosen randomly from the available ten curves, the resulting average does not differ appreciably from the solid line, i.e., already five curves (i.e., five different configurations of the matrix) are enough to define an average that no

longer depends on the configuration of the finite sample of the matrix in the simulation volume. The solid lines in Fig. 2 and all the subsequent results for $D(t)$ or $W(t)$ were obtained, however, by averaging over at least ten curves. Notice, from Fig. 2, that the dispersion of the ten curves for $D(t)$ around the final average is somewhat smaller for $K = 500$ than for $K = 100$. This comes from the fact that when the particles repel each other more strongly, the frozen configuration of fixed particles tends to show a more "homogeneous" distribution of "pore" sizes and structures, whereas at smaller K, the weaker correlation between particles before the matrix is frozen leads to a broader distribution of pores, which may not

be sufficiently well represented by the finite simulation cell.

The results in Fig. 2 show the decay of $D(t)$ from its initial value $D(0) = D^0$ towards its asymptotic value, which we denote by D^L. The truly asymptotic long-time regime, however, is out of the reach of our computer simulation runs. At such long times, a given tracer particle shoud have diffused over many times the mean distance between particles $l \sim n^{-\frac{1}{3}}$. Thus long-times mean $t \gg \tau_I$, with $\tau_I \sim l^2/D^0$. In units of the scaling time $t_0 \equiv \sigma^2/D^0$, this "interaction" time is $\tau_I/t_0 \sim (l/\sigma)^2$. For the systems in Fig. 2, for which $l \sim 10\sigma$ (see Fig. 1), $\tau_I/t_0 \sim 10^2$. Thus the longest times plotted in Fig. 2
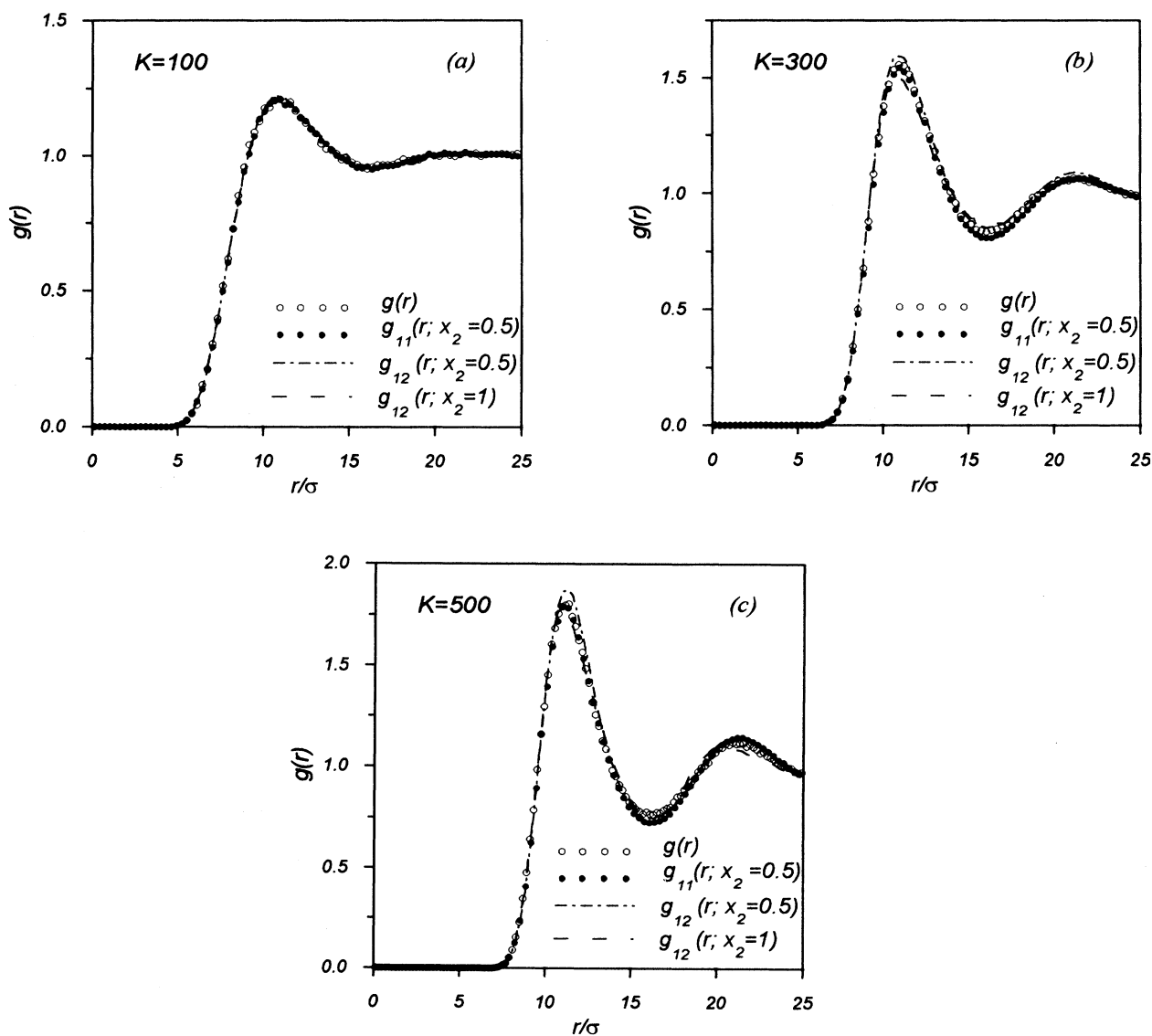

FIG. 1. Brownian dynamics results for the radial distribution functions $g(r)$ for a monodisperse Brownian fluid ($x_2 = 0$, empty circles), for $g_{11}(r)$ and $g_{12}(r)$ for the case in which half of the particles constitute the porous matrix ($x_2 = 0.5$, full circles and dot-dashed curves, respectively), and $g_{12}(r)$ for the case in which all the particles, except the tracer particle (species 1), constitute the matrix ($x_2 = 1$, dashed line). These results correspond to $z = 0.15$, $\phi = 4.4 \times 10^{-4}$, and $K = 100$ (a), 300 (b), and 500 (c). In these three cases, the various $g_{\alpha\beta}(r)$ are numerically almost indistinguishable.
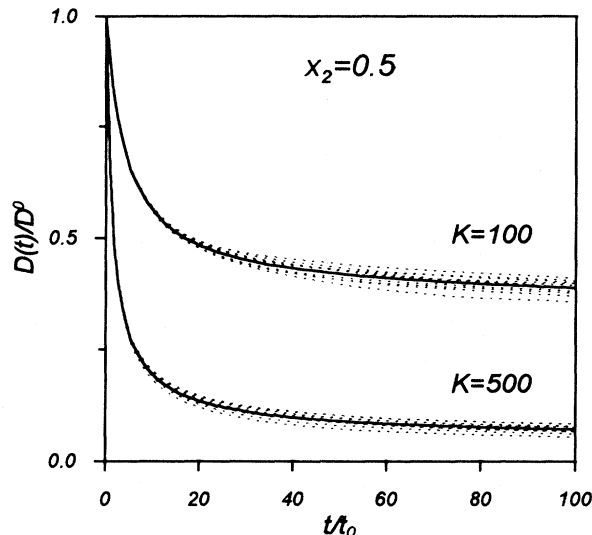
FIG. 2. BD results for the time-dependent diffusion coefficient $D(t)$ scaled with the free-diffusion coefficient D^0 as a function of time, scaled with $t_0 \equiv \sigma^2/D^0$, corresponding to $x_2 = 0.5$, and $K = 100$ and 500. Each solid line is the average of the ten dashed lines clustered around it. Each of these dashed lines corresponds to a given random spatial configuration of the particles constituting the porous matrix.

correspond to times comparable to τ_I. It is clear, however, that already in this time interval, the main decay of $D(t)$ has occurred, although a weaker, longer-lived relaxation still occurs at times $t \geq \tau_I$. We notice that this slower decay is more pronounced at larger values of K and even more so when the fraction of fixed particles increases ($x_2 \to 1$). Although this is an important and interesting effect that deserves further discussion, for the time being we shall focus, however, on the opposite regime, corresponding to the short times, where the most dramatic effect of the collisions occur and the tracer explores distances comparable to the size of the pore or smaller. From Fig. 2 we can see that the relaxation time associated with the rapid initial decay of $D(t)$ is of the order of a fraction of τ_I, let us say, of about $\tau_I/5$. In what follows, we shall restrict our analysis to this time interval (i.e., to times $t \leq 20t_0$ for the particular systems analyzed here).

Let us start our discussion by looking at the initial behavior of $D(t)$. This is better illustrated by looking instead at the mean squared displacement $W(t)$, which we present in Fig. 3. Here we compare in one case [Fig. 3(a)] $W(t)$ for a fixed interaction ($K = 300$), varying the fraction of the fixed particles $x_2 = 0, 0.5$, and 1. In the other case, we keep x_2 fixed at $x_2 = 0.5$ and see the effect of varying the interaction parameter ($K = 100, 300$, and 500). Let us first notice the very early behavior of $W(t)$, which in all cases approaches free diffusion as $t \to 0$, i.e., $W(t) \approx D^0 t$. Thus this initial time regime represents the motion of the tracer particle in the "center" of an average cage (or "pore"), diffusing over distances comparable to its hard-sphere size. After this free-diffusion regime, the effect of the interparticle interactions starts to be-

come important and it is only then that these departures from free diffusion amplify the differences between different systems and conditions. The extent of this early departure from free diffusion clearly depends on how soft or rigid the cage is, i.e., on x_2 [Fig. 3(a)], and on the strength of the repulsion, i.e., on K [Fig. 3(b)]. The dependence on x_2 and K of the early departure of $W(t)$ from free diffusion is better explained by normalizing $W(t)$ by its free-diffusion value $D^0 t$, i.e., by plotting $D(t)/D^0$. To illustrate this, in Fig. 4 we present our results in terms of $D(t)$ for the three regimes of composition ($x_2 = 0, 0.5$, and 1) and the three values of K ($K = 100, 300$, and
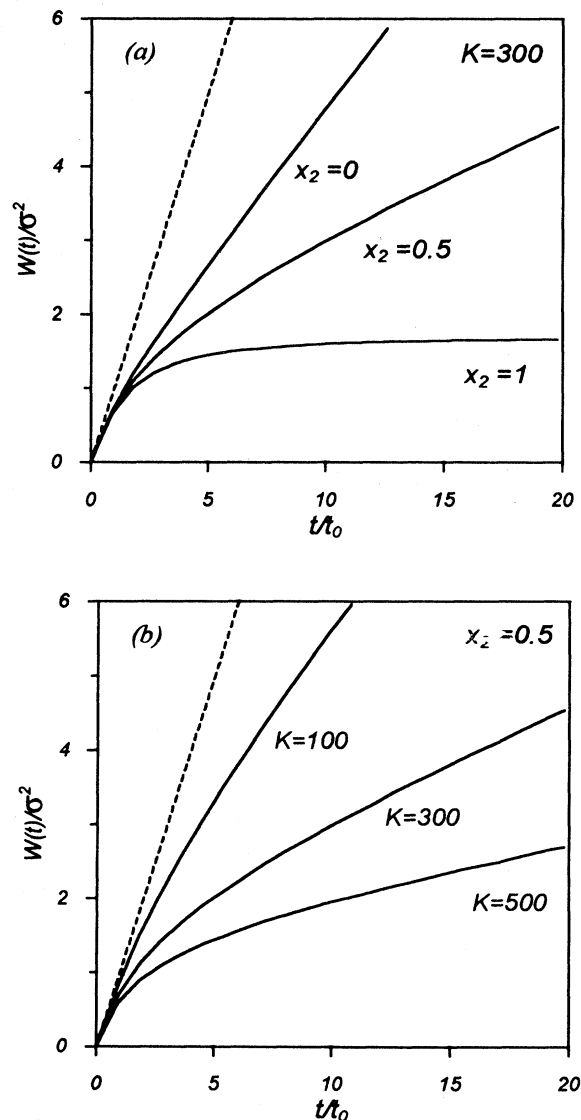

FIG. 3. BD results for the mean squared displacement, scaled with the squared hard-sphere diameter σ^2, as a function of time for (a) a fixed value of the Yukawa amplitude parameter K ($K = 300$) and three values of the fractional concentration of fixed particles x_2 (= 0, 0.5, and 1) and (b) for fixed $x_2 = 0.5$ and $K = 100, 300$, and 500. The dashed line corresponds to free diffusion $W(t) = D^0 t$.

500). Although this is essentially the same information already displayed in Fig. 3, plotting it in this manner allows us to observe still another important feature of our simulation results regarding the short-time regime.

As apparent in Fig. 4, for a given value of K, the initial decay of $D(t)$ as a function of time happens to be the same for the three cases $x_2 = 0, 0.5$, and 1. This common initial behavior, however, does depend on the strength of the interaction, which is faster for larger values of K. The reason for this is that this short-time regime corresponds to the times in which the effects of the interactions of the tracer with its cage are first manifested. The independence of this initial decay on the ratio of fixed to mobile particles indicates that in this short-time regime the tracer cannot yet distinguish between a rigid ($x_2 = 1$) or a completely soft ($x_2 = 0$) cage of surrounding particles.

At longer times, however, the three curves ($x_2 = 0, 0.5$, and 1) clearly depart from each other and show the extent of the effect of the rigidity of the surroundings on the average motion of the tracer particle. Of course, the more rigid the cage is (i.e., the larger x_2), the larger the friction and hence the smaller the effective time-dependent diffusion coefficient $D(t)$. This could already be seen from the mean squared displacement $W(t)$ in Fig. 3(a), which contains the same information as in Fig. 4(b). Clearly, in this case ($K = 300$), the completely rigid matrix ($x_2 = 1$) almost confines the tracer particle [see Fig. 3(a)]. Of course, this effect is still stronger for higher values of K, as we can appreciate in the lower curve of Fig. 4(c), in which case $D(t)$ approaches zero for times $t \sim \tau_I$. In Fig. 4 we have also plotted the theoretical prediction for the linear approximation $D(t)/D^0 \approx 1 + \frac{1}{2}(n\beta D^0 A)t$ with
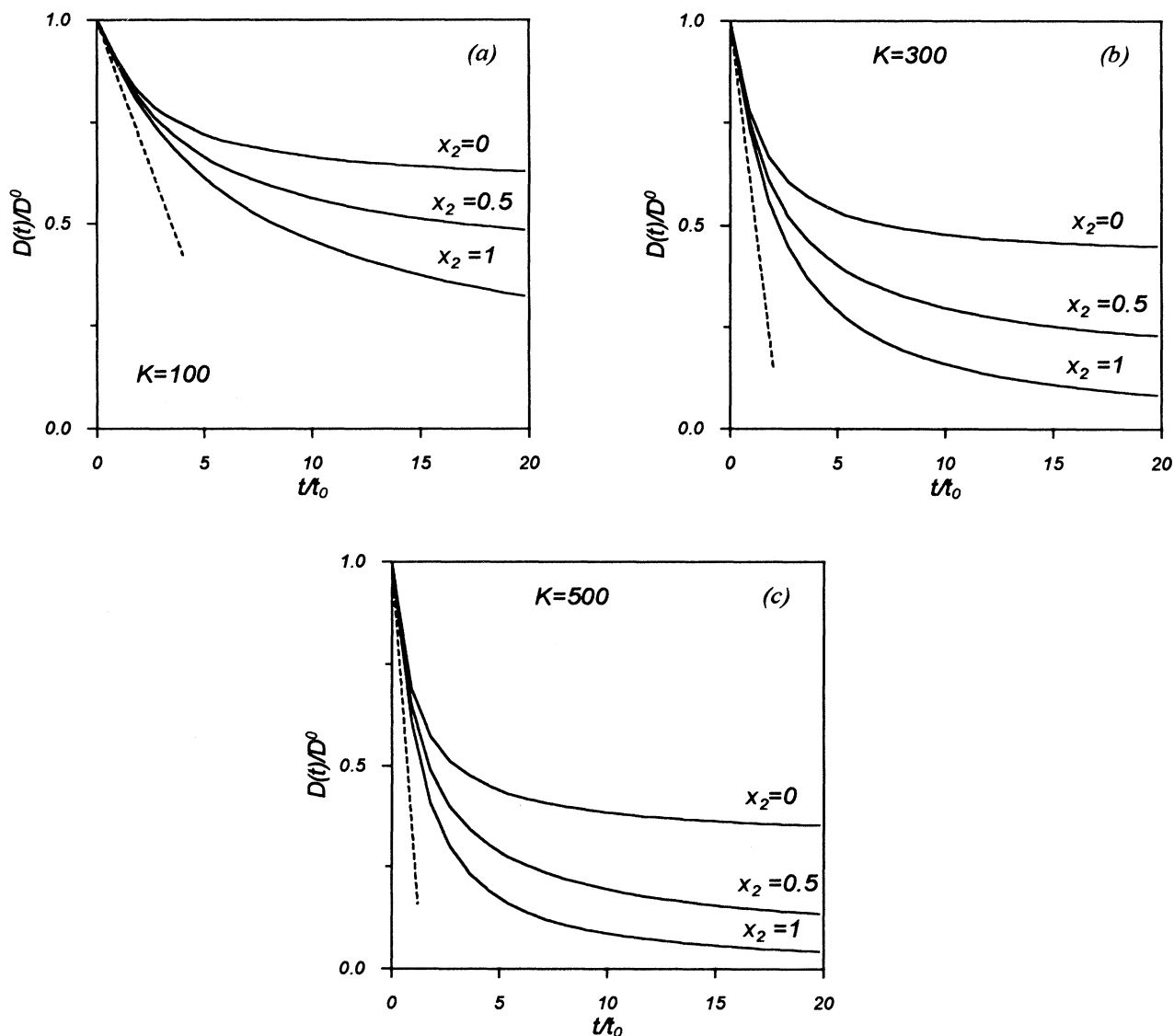

FIG. 4. BD results for the time-dependent diffusion coefficient $D(t)$ as a function of time for $x_2 = 0$, 0.5, and 1 and (a) $K = 100$, (b) $K = 300$, and (c) $K = 500$. The dashed line corresponds to the linear approximation $D(t)/D^0 = 1 - \frac{1}{2}(n\beta D^0 A)t$ in Eq. (5.13).

A given by Eq. (5.10) below, which is an integral of the radial distribution function times the derivative of $u(r)$. This theoretical result will be discussed later. Here we only mention that this is an exact result and the straight line in Fig. 4 was evaluated using the computer-simulated $g(r)$. Clearly, the linear approximation is accurate only within a very short initial time interval (of the order of t_0). Very soon, the three curves depart from the straight line, but still remain together until the effect of the rigidity of the cage manifests itself. This happens within a time of about a few (~ 3) times t_0.

V. THEORETICAL INTERPRETATION

From a theoretical point of view, one would like to understand these and other structural properties (static and dynamic) of a fluid system permeating a porous material in terms of the microscopic properties of the different components, i.e., the interaction between mobile particles and between them and the walls of the pores, the porosity of the matrix, the mobile particle concentration, etc. The development of a microscopic theory describing phenomena such as the motion of a Brownian particle in a porous medium is an interesting and challenging problem in itself, which requires a careful consideration of a variety of effects. However, for the simplified model considered in this work we may attempt, as a simple approach, to make use of theories for tracer-diffusion phenomena in suspensions of mixtures of colloidal particles, in the limit in which the free-diffusion coefficient of one species goes to zero in a way similar to the way our BD calculations were performed. In this work we compare our BD results above with the predictions of two independent theories, which express the MSD of tracer particles in a colloidal mixture in terms of the static properties of the suspension. Both theoretical approaches are now described and adapted to the problem under consideration.

In one of the theories, cast in terms of a generalized Langevin equation [20–22], the diffusion of tracer particles in a colloidal mixture is described by a generalized Langevin equation of the form

$$M\frac{d\mathbf{V}(t)}{dt} = -\zeta_T^0 \mathbf{V}(t) + \mathbf{f}(t)$$
$$- \int_0^t \Delta\zeta(t - t')\mathbf{V}(t)dt' + \mathbf{F}(t). \quad (5.1)$$

The effect of the direct interactions between particles gives rise to the memory term and its corresponding fluctuating force $\mathbf{F}(t)$. Thus $\Delta\zeta(t)$ is a time-dependent friction function, which, as explained elsewhere [22], can be written in general as

$$\Delta\zeta(t) = \frac{k_B T}{(2\pi)^3} \sum_{\alpha,\beta,\gamma}^{\nu} \int d^3k\, k_z^2\, n_\alpha\, h_{T\alpha}(k)\, \frac{[\mathbf{S}^{-1}(k)]_{\alpha\beta}}{(n_\alpha n_\beta)^{1/2}}$$
$$\times \chi_{\beta\gamma}^*(k,t)\, n_\gamma\, h_{T\gamma}(k), \quad (5.2)$$

where $h_{T\alpha}(k)$ is the Fourier transform of the total correlation function $h_{T\alpha}(r) = g_{T\alpha}(r) - 1$ between particles

of species T and α in a mixture of ν species, $\mathbf{S}(k)$ is the matrix of partial static structure factors, and $\chi_{\alpha\beta}^*(k,t)$ is given by

$$\chi_{\alpha\beta}^*(k,t) = \chi_T(k,t)\,\chi_{\alpha\beta}(k,t)$$
$$= \exp(-D_T^0 k^2 t)\{\exp[-k^2 \mathbf{L}\sigma^{-1}(k)t]\}_{\alpha\beta}, \quad (5.3)$$

where $L_{\alpha\beta} = D_\alpha^0 n_\alpha \delta_{\alpha\beta}$ and $\sigma_{\alpha\beta}(k) = n_\alpha^{1/2} n_\beta^{1/2} S_{\alpha\beta}(k)$. Equations (5.2) and (5.3) involve a number of approximations [22], which have been referred to as the *Fick plus decoupling approximation* (FDA).

In order to apply this result to the quenched system studied in this work, we consider, as in our BD calculations, a monodisperse colloidal suspension conceived as two subsystems of fractional concentrations x_1 and x_2. Since the static properties required as input depend only on the direct interactions, which in this case are identical for both species, the *equilibrium* radial distribution functions between particles of the two species are, of course, identical and equal to the RDF $g(r)$ of the monodisperse system of concentration n. However, in our partially quenched system, we need to take this property as an additional assumption, which, according to the simulated results in Sec. III for the radial distribution functions, is found to be quite justified. Thus, assuming that $g_{11}(r) = g_{12}(r) = g_{22}(r) = g(r)$ is indeed a reasonable assumption, which cannot be the source of possible inaccuracies of the quantitative results calculated from Eq. (5.2). In this manner, the seemingly complicated expression in this equation simplifies considerably for the particular circumstances that concern us, namely, when we have two species that only differ in the value of their free-diffusion coefficient (i.e., $D_1^0 = D^0$ and $D_2^0 = 0$), and the resulting expression for the time-dependent friction function of a tracer of species 1 is

$$\Delta\zeta(t) = \frac{k_B T}{(2\pi)^3} \int d^3k\, k_z^2\, h^2(k)\, \exp\left(-k^2 D^0 t\right)$$
$$\times \left\{ \frac{n_1}{[1 + n_2 h(k)][1 + n h(k)]} \right.$$
$$\times \exp\left[-k^2 D^0 t\left(\frac{1 + n_2 h(k)}{1 + n h(k)}\right)\right]$$
$$\left. + \frac{n_2}{1 + n_2 h(k)} \right\}. \quad (5.4)$$

This expression interpolates between two interesting limiting cases. In the limit $n_2 \to 0$, it reduces to

$$\Delta\zeta(t) = \frac{k_B T}{(2\pi)^3} n \int d^3k\, k_z^2\, \frac{h^2(k)}{1 + n h(k)}$$
$$\times \exp\left(\frac{-k^2 D^0 t}{1 + n h(k)}\right) \exp\left(-k^2 D^0 t\right). \quad (5.5)$$

This is the particular FDA result for self-diffusion in a monodisperse suspension and happens to coincide with Hess and Klein's mode-mode coupling expression [14]. In the opposite limit $n_1 \to 0$, Eq. (5.4) reduces to

$$\Delta\zeta(t) = \frac{k_B T}{(2\pi)^3} n \int d^3k\, k_z^2\, \frac{h^2(k)}{1 + n h(k)} \exp\left(-k^2 D^0 t\right),$$
$$(5.6)$$

which can be viewed as Eq. (5.5) with the collective propagator $\exp\{-k^2 D^0 t/[1 + nh(k)]\}$ of the immobile particles of species 2 set equal to 1, due to the vanishing of their free-diffusion coefficient.

Equation (5.4) now requires the RDF $g(r)$ of the equilibrium monodisperse system. In order to avoid additional sources of inaccuracies rather than employing any statistical mechanical approximation for this function, in the specific calculations reported below we shall employ as the static input the Brownian dynamics results. As a mere numerical aid to calculate the Fourier transform $h(k)$, however, the simulated results were fitted using the rescaled mean spherical approximation [23], as explained in Ref. [16]. This reference also contains details on the numerical procedure, which we also follow here, to calculate the mean squared displacement starting from $\Delta\zeta(t)$.

The second theory, referred to as the *single exponential* (SEXP) *approximation* [15,24–26], also provides a general expression for the mean squared displacement of a particle of species α in a mixture of ν colloidal species [26]. By construction, the short-time expansion of such expression is exact up to terms of order t^3. As applied to our binary mixture, upon the introduction of the same assumption concerning the identity of the partial RDF's and setting $D_2^0 = 0$, one obtains the following result for the mean squared displacement of a mobile particle:

$$W(t) = D^L t + \tau(D^0 - D^L)(1 - e^{-t/\tau}), \qquad (5.7)$$

where

$$\frac{D^L}{D^0} = 1 - \frac{nA^2}{(2 - x_2)B + nC} \qquad (5.8)$$

and

$$\tau = \frac{k_B T A}{D^0[(2 - x_2)B + nC]}, \qquad (5.9)$$

with

$$A = \int d^3 r\, g(r) \left(\hat{\mathbf{k}} \cdot \boldsymbol{\nabla}\right)^2 u(r), \qquad (5.10)$$

$$B = \int d^3 r\, g(r) \left[\left(\hat{\mathbf{k}} \cdot \boldsymbol{\nabla}\right) \boldsymbol{\nabla} u(r)\right]^2, \qquad (5.11)$$

and

$$C = \int\!\!\int d^3 r\, d^3 r'\, g^{(3)}(\mathbf{r}, \mathbf{r}') \left(\hat{\mathbf{k}} \cdot \boldsymbol{\nabla}\right) \left(\hat{\mathbf{k}} \cdot \boldsymbol{\nabla}'\right)$$
$$\times \left(\boldsymbol{\nabla} \cdot \boldsymbol{\nabla}'\right) u(r) u(r'). \qquad (5.12)$$

As an additional simplification, terms containing the three-particle distribution function $g^{(3)}(\mathbf{r}, \mathbf{r}')$, which are quadratic in the number densities, are neglected. Here too we take the BD results for $g(r)$ as the static input required in the concrete application of these expressions. The results of this and the previous theory are now presented and compared with the BD calculations. This is done in Fig. 5.

At this time, let us mention that the short-time expansion of the expression in Eq. (5.7) can be written, in terms of $D(t)$, as

$$\frac{D(t)}{D^0} = 1 - \frac{1}{2}(n\beta D^0 A)t$$
$$+ \frac{1}{6}n(\beta D^0)^2[(2 - x_2)B + nC]t^2 + \cdots, \qquad (5.13)$$

with A, B, and C given by Eqs. (5.10)–(5.12). The first thing to notice is that, although the full expression for $D(t)$ in Eq. (5.10) is an approximation, its expansion is exact up to terms of order t^2 for $x_2 = 0$. Equation (5.13), however, predicts that the very initial slope of $D(t)$ as a function of time is independent of x_2. This prediction is accurately followed by our BD results, as discussed before in Fig. 4, although the expansion in Eq. (5.13) up to linear order is only good at very short times. Furthermore, at slightly longer times, where the quadratic term in Eq. (5.13) becomes important, the dependence on x_2 of the initial curvature is also not large, as also observed from Fig. 4. As we see now, the initial behavior predicted by Eq. (5.13), which is contained in the full SEXP expression in Eq. (5.7), agrees very accurately with the BD simulations for all values of K and x_2 studied, in spite of the neglect of the term nC, as we can see from Fig. 5. In comparison, the behavior of the FDA results for $D(t)$ does not satisfy exactly the exact moment conditions in Eq. (5.13). In particular, the initial slope of $D(t)/D^0$ is still given by $\frac{1}{2}(n\beta D^0 A')$, with A' given by the same expression for A in Eq. (5.10), but with $u(r)$ replaced by $-k_B T c(r)$, where $c(r)$ is the Ornstein-Zernike direct correlation function. This difference explains the early departure of the FDA results from the BD simulations at very short times. Let us now discuss other general features of the results in Fig. 5.

First of all, let us compare our BD results for $D(t)$ with the corresponding calculations from both theories for the case in which all the particles are mobile, i.e., the case of self-diffusion. This comparison is presented in Fig. 5(a) for the two extreme values of the coupling constant K, namely, $K = 100$ and 500. As one can see, both theories reproduce very well the BD results at short and intermediate times, with some deviation at longer times, which is more pronounced for the more strongly interacting system. These conclusions are only consistent with the results of similar calculations in the context of the description of self-diffusion in monodisperse suspensions [16] and here we present them as a reference for the new results in the same figure. Thus, in Fig. 5(b) we illustrate the typical conditions that we wish to study, namely, the case in which half of the total number of particles of the system are kept fixed and the other half follow their Brownian motion. We observe that both theories predict essentially the same behavior for $D(t)$ as the BD simulations. There is even a very good quantitative agreement for not too high values of the coupling constant. Let us notice, however, that although in this regime ($x_2 \sim 0.5$) the FDA results seem to perform quantitatively better than the results of the SEXP approximation and that this was also observed for other values of the coupling parameter K not shown in the figure, this apparent advantage of the FDA may only be accidental.

In going from Fig. 5(a) to Fig. 5(b) one should also take into account that in the process of increasing x_2 at

fixed K the friction on the tracer increases not because the interaction with the other particles becomes stronger or because the tracer particle interacts with more particles (since n remains fixed). This increase in the friction, and the corresponding decrease in $D(t)$, is only due to the increase in the rigidity of the surrounding cage, which is formed, as x_2 increases, by a larger number of fixed particles. We know, on the other hand, that when the friction increases due to an increase in the coupling parameter, even without the effect of any rigidity of the cage [$x_2 = 0$, as in Fig. 5(a) and in Ref. [16]], the quantitative accuracy of the two theories, and their mutual agreement, deteriorates. Thus the results in Fig. 5(b) illustrate the extent of such a disagreement when we have an intermediate situation. We can advance, however, that if the rigidity of the cage increases even further, the friction will be so large due to this effect (an effect that neither of the two theories was meant to describe) that one should not expect any form of quantitative agreement. This is what we found at the values of K we chose to consider here and this is what is illustrated in Fig. 5(c), corresponding to the limit of complete rigidity of the cage. Let us first look at the smallest coupling, $K = 100$. If we were to compare the results of the two theories and the BD simulations for $K = 100$ in Figs. 5(a)–5(c), we would conclude that the SEXP approximation exhibits remarkably better quantitative agreement than the FDA. This, however, seems to reverse at larger values of the coupling parameter K. In fact, already for $K \sim 300$, the SEXP approximation breaks down, leading to the unphysical result $D^L < 0$, where D^L is the asymptotic long-time value of $D(t)$. This is illustrated by the results for $K = 500$ in
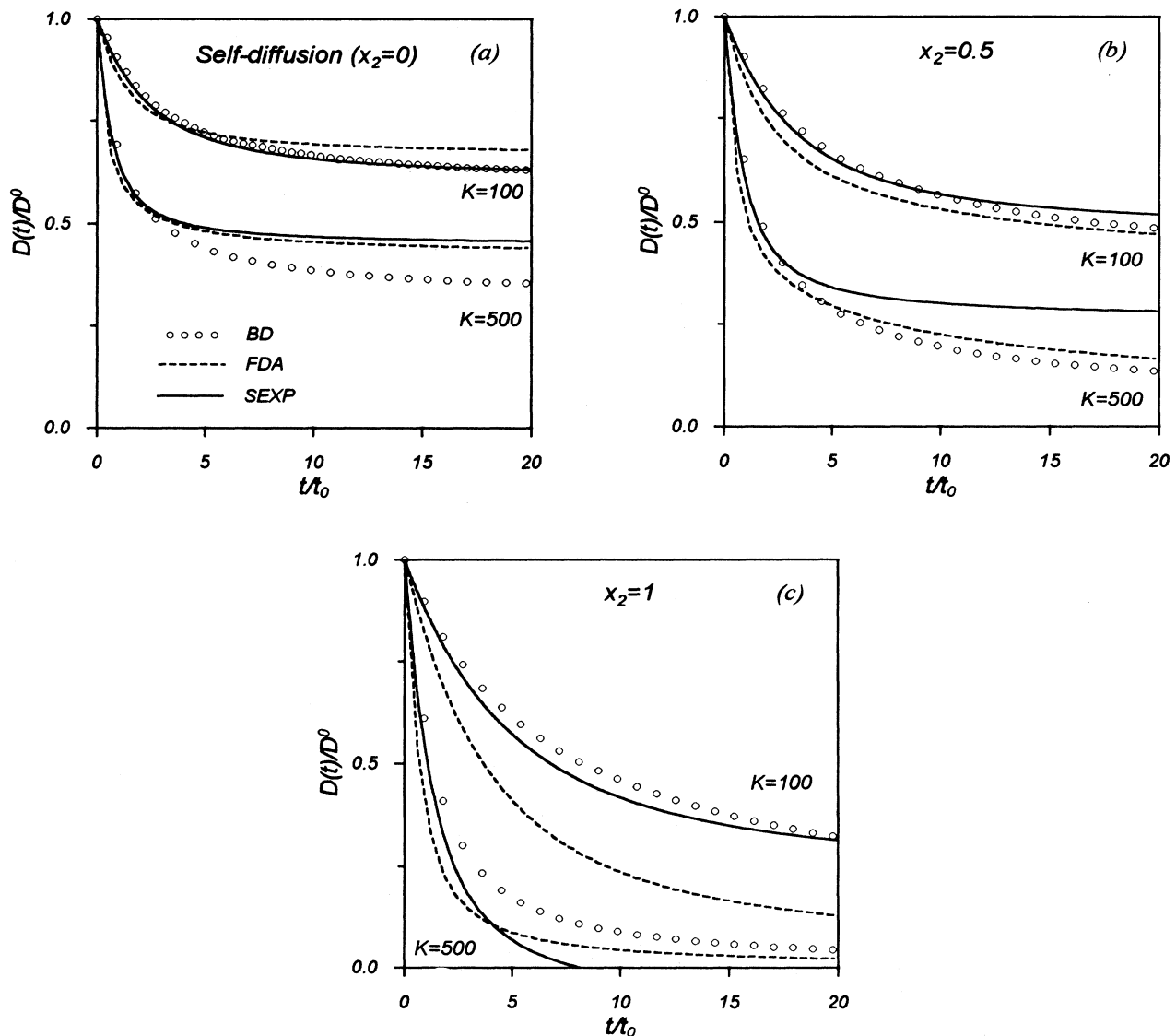

FIG. 5. Comparison of the results of the SEXP approximation (solid lines) and the FDA (dashed lines) for $D(t)$ with the Brownian dynamics results (empty circles) for two values of K (= 100 and 500) and three values of the fractional concentration of mobile particles $x_2 = 0$ (a), 0.5 (b), and 1 (c).

Fig. 5(c), where one can see that the SEXP $D(t)$ vanishes at $t \sim 7t_0$ and becomes negative after that. In comparison, the FDA results for $D(t)$ can never become negative. However, their apparent better agreement with the simulations results cannot be but accidental, considering the results in the same figure for $K = 100$.

VI. DISCUSSION

The extreme case $x_2 = 1$, $K = 500$, just referred to, was presented mostly for completeness and to illustrate the degree of failure of the two theories when they are applied to really extreme conditions. In reality, this state corresponds to the case in which the tracer particle is completely trapped by its totally rigid cage. This effect can be seen already for $K = 300$ [see Fig. 3(a), lower curve], where the mean squared displacement almost levels to a constant value, which is of the order of only a few squared diameters σ^2. The theoretical description of this type of caging, with an extremely small probability of hopping to neighboring cages, should be attempted with other approaches such as percolation theory [27]. Nevertheless, the comparison of the theoretical results with the BD simulations in Fig. 5 indicates that more improved versions of these two theoretical approaches, along with their application in the opposite regime, namely, when there is no complete trapping, such as for values of $K < 300$ for $x_2 \approx 1$, or even for larger couplings when $x_2 \approx 0.5$, may still be quite useful.

The results presented in this paper thus, on the one hand, provide a description, based on the Brownian dynamics simulations, of the self-diffusion in a fluid of interacting Brownian particles permeating a model porous matrix. These results illustrated some features associated with the short-time regime, which can be well understood on the basis of their comparison with what has been learned in the context of self-diffusion in model colloidal suspensions in the bulk. On the other hand, the availability of these simulation results also allowed us to assess the possible use of theoretical approaches developed to describe tracer diffusion in colloidal mixtures, adequately adapted, or extrapolated, to the problem at hand. We can conclude that these theories, as they stand, turn out to be quite useful when we do not get very far from the regime in terms of K and x_2 for which they were devised, namely, for a more reduced range of K when x_2 is increased from its self-diffusion value $x_2 = 0$. Here we also illustrated the opposite regime, of high rigidity and large couplings, where the very reduced effective porosity of the system does not allow the tracer particles to diffuse away from their initial pore. In this regime we conclude that there is a need for other approaches to attempt a quantitative theoretical description of the BD results.

ACKNOWLEDGMENTS

[1] J. M. Drake and J. Klafter, Phys. Today, **43** (5), **46** (1990).

[2] M. Sahimi, Rev. Mod. Phys. **65**, 1393 (1993).

[3] P. Levitz, G. Ehret, S. K. Sinha, and J. M. Drake, J. Chem. Phys. **95**, 6151 (1991).

[4] S. Torquato, Physica A **207**, 79 (1994).

[5] R. Evans, U. M. B. Marconi, and P. Tarazona, J. Chem. Soc. Faraday Trans. 2 **82**, 1763 (1986); V. Vlachy and A. D. J. Hayment, Chem. Phys. Lett. **146**, 32 (1988); P. González-Mozuelos, J. Alejandre, and M. Medina-Noyola, J. Chem. Phys. **95**, 8337 (1991).

[6] E. Lomba, J. A. Given, G. Stell, J. J. Weis, and D. Levesque, Phys. Rev. E **48**, 233 (1993); C. Vega, R. D. Kaminsky, and P. A. Monson, J. Chem. Phys. **99**, 3003 (1993).

[7] W. D. Dozier, J. M. Drake, and J. Klafter, Phys. Rev. Lett. **56** 197 (1986).

[8] M. Sahimi, J. Chem. Phys. **96**, 4718 (1992); M. Sahimi and V. L. Jue, Phys. Rev. Lett. **62**, 629 (1989).

[9] I. C. Kim and S. Torquato, J. Chem. Phys. **96**, 1498 (1992); S. Torquato, ibid. **95**, 2838 (1991).

[10] G. Viramontes-Gamboa, J. L. Arauz-Lara, and M. Medina-Noyola, Phys. Rev. Lett. **75**, 759 (1995).

[11] D. L. Ermak and J. A. McCammon, J. Chem. Phys. **69**, 1352 (1978).

[12] K. J. Gaylor, I. K. Snook, and W. J. van Megen, J. Chem. Soc. Faraday Trans. 2 **76**, 1067 (1980).

[13] P. N. Pusey and R. J. A. Tough, in *Applications of Photon Correlation Spectroscopy*, edited by R. Pecora (Plenum, New York, 1985).

[14] W. Hess and R. Klein, Adv. Phys. **32**, 173 (1983).

[15] J. L. Arauz-Lara and M. Medina-Noyola, J. Phys. A **19**, L117 (1986).

[16] G. Nägele, M Medina-Noyola, R. Klein, and J. L. Arauz-Lara, Physica A **149**, 123 (1988).

[17] R. Krauze, G. Nägele, D. Karrer, J. Schneider, R. Klein, and R. Weber, Physica A **153**, 400 (1988).

[18] M. P. Allen and D. J. Tildesley, *Computer Simulation of Liquids* (Oxford Science, New York, 1987).

[19] J. P. Hansen and I. R. McDonald, *Theory of Simple Liquids*, 2nd ed. (Academic, New York, 1986).

[20] M. Medina-Noyola and A. Vizcarra-Rendón, Phys. Rev. A **32**, 3596 (1985).

[21] M. Medina-Noyola, Faraday Discuss. Chem. Soc. **83**, 21 (1987).

[22] G. Cruz de León, M. Medina-Noyola, O. Alarcón-Waess, and H. Ruiz-Estrada, Chem. Phys. Lett. **207**, 294 (1993).

[23] J. P. Hansen and J. B. Hayter, Mol. Phys. **46**, 651 (1982).

[24] J. L. Arauz-Lara, Ph.D. thesis, Centro de Investigación y de Estudios Avanzados del IPN, 1985 (unpublished).

[25] J. L. Arauz-Lara and M. Medina-Noyola, Physica A **122**, 547 (1983).

[26] J. L Arauz-Lara, H. Ruiz-Estrada, M. Medina-Noyola, G. Nägele, and R. Klein, Prog. Colloid Polym. Sci. **84**, 377 (1991); G. Nägele, M. Medina-Noyola, J. L. Arauz-Lara, and R. Klein, ibid. **73**, 5 (1987).

[27] M. Sahimi, *Applications of Percolation Theory* (Taylor and Francis, London, 1994).